2024 IEEE International Conference on Robotics and Automation (ICRA 2024)
May 13-17, 2024. Yokohama, Japan

Mechanical Design and Kinematics of a Multimodal Two-wheeled Robot

Botian Sun, Qinglin Lang, Minghe Li, Xuefeng Wang

***Abstract*— A two-wheeled vehicle has a compact structure and high mobility in crowded and complex environments, which has been widely used in urban logistics. The bicycle and self-balancing vehicle are the two main modes of the two-wheeled vehicle, and their combination allows for good balance-control stability at both high and low speeds. Four control inputs by two steerable driving wheels are required to implement transformations between the two modes due to the difference in their configuration spaces. However, the control inputs are redundant for planar motions, which results in an over-constraint of the vehicle. In this work, a two-wheeled robot with an additional structural degree of freedom (DOF) is designed to balance inputs and DOFs to avoid over-constraint. A transition mode based on oblique vehicle motions is used to bridge the transformation of the bicycle and self-balancing vehicle modes. A general kinematic model is developed for the two-wheeled robot's planar motions, and the three modes' kinematics are special cases with particular servo constraints. Structural DOF control laws are developed and experimentally validated on a prototype robot. Smooth transformations of the multimodal motions are also validated by using the prototype.**

I. INTRODUCTION

Two-wheeled vehicles have the advantages of high mobility, agility, and reliability, and the compact structure is suitable in crowded environments such as indoors and in urban areas. Bicycles and self-balancing vehicles are two main modes of two-wheeled vehicles, which continuously attract the attention of researchers [1][2].

The bicycle is, by nature, a statically unstable system with two wheels placed along the longitudinal axis of the frame. It can be stabilized by steering control of the front wheel or even self-stabilized without active control at high speeds [3], but it has poor stability at low speeds [4]. Unlike the bicycle, the self-balancing vehicle is actuated by two co-axial wheels, whose moving direction is the same as the falling direction. Therefore, the self-balancing vehicle has good balance-control stability at low speeds [5], but it generally does not drive fast to avoid severe safety issues once it falls [6]. A two-wheeled vehicle robot that transforms between the bicycle and self-balancing vehicle modes can achieve a wider speed range of balancing control.

When a two-wheeled vehicle is balanced, its spatial movements are reduced to planar motions. Planar motions of general wheeled vehicles were comprehensively studied [7], and the number of independent control inputs (simplified as control inputs) was defined as the degree of maneuverability, δ_M, which includes the degree of mobility δ_m and the degree of steerability δ_s with $\delta_M = \delta_m + \delta_s$, where δ_m and δ_s indicate DOFs of the vehicle body without wheel reorientation and that of wheel steering, respectively. The bicycle has a steerable wheel and a non-steerable driving wheel, with $\delta_s = 1, \delta_m = 1$. The self-balancing vehicle does not have steerable wheels but has two independent driving wheels to implement forward motion and rotation so that $\delta_s = 0, \delta_m = 2$. Although the bicycle and self-balancing vehicle own only two DOFs of planar motions, switching between the two modes requires three-DOF planar motions of the two-wheeled vehicle.

The three-DOF planar motion of wheeled robots can be achieved using multiple steerable regular wheels or specially designed wheels, such as omnidirectional and Mecanum wheels [8]. Regular wheels with elastic rubber tires are widely used due to good terrain adaptation, high reliability, and easy integration with hub motors. Three-DOF planar motions of a two-wheeled vehicle with regular wheels are usually realized by a combination of two degrees of steerability and one degree of mobility[9][10][11], which is called the dual-steering bicycle. However, the dual-steering bicycle cannot be transformed into the self-balancing vehicle mode. Regarding configuration space, the degrees of mobility of the dual-steering bicycle and self-balancing vehicle are different since one of the bicycle's wheels is passively driven, resulting in a motion singularity in the self-balancing vehicle mode.

To implement the transformation between the two modes by three-DOF planar motions, four control inputs, including driving and steering actuators of the two wheels, are required in the two-wheeled robot. However, the number of control inputs exceeds the DOF of planar motions, which introduces over-constraint that can cause wheel slipping and frame shaking [12][13], affecting the maneuverability. Speed control is a commonly used strategy to handle the over-constraint problem [14][15]. The instant center method was used to solve non-slipping wheel speeds for rotational motions [16][17]. By assuming a virtual linkage between each of the two steerable driving wheels, a control algorithm was developed for general over-constraint wheeled robots [18]. However, the effects of over-constraint cannot be eliminated by the control algorithm due to cumulative errors in motor control, measurement errors in encoders, tolerances in wheel radii, and rough road surfaces [13]. A linkage with a linear sensor between the front and rear pairs of wheels was introduced to solve the over-constraint of a four-wheeled vehicle [13]. In other types of robots that suffer from over-constraint problems, such as the human-machine interactive mechanism of upper limb exoskeletons, additional joints are used to balance numbers of the DOF and control inputs [19][20][21].

The authors are with the Department of Advanced Manufacturing and Robotics, College of Engineering, Peking University, Beijing, China (Corresponding author: Xuefeng Wang)(e-mail: sunbotian@pku.edu.cn, langql@stu.pku.edu.cn, Lminghe@outlook.com, wang_xf@pku.edu.cn)

The mechanical approach is used here to avoid the over constraint of the two-wheeled robot with four inputs.

In this work, a multimodal two-wheeled robot with two steerable driving wheels is designed to achieve 3-DOF planar motions and smooth transformation between bicycle and self-balancing vehicle modes. A slider joint is incorporated into the robot's design, and the robot's workspace owns three planar motion DOFs and one structural DOF. Three control inputs are used to control the planar motion, and the other input is used to control the structural DOF so that the over-constraint problem is physically avoided by the mechanism design. A general kinematic model of the proposed two-wheeled robot is established, and forward and inverse kinematics of three motion modes, including the bicycle, self-balancing vehicle, and oblique vehicle, are obtained by introducing particular servo constraints in the general kinematic model. The oblique vehicle mode is used as a bridge to connect the bicycle and self-balancing vehicle modes since there are intersections between its servo constraint and those of the other two modes. Experimental results show that the over-constraint problem is solved, and smooth transformations among the three modes can be realized with stable control of the structural DOF.

In the following, Section II describes the mechanical and electrical design of the robot. Forward and inverse kinematics and mode transformations of the system are established in Section III. Section IV shows the experimental results of the multimodal motions by a prototype of the two-wheeled robot.

II. Design

A. Mechanical Design

The multimodal two-wheeled robot proposed in this work has three modules: the vehicle body module, the front motion module, and the rear motion module, as shown in Fig. 1. The vehicle body module comprises a frame, a rail-slider mechanism, and front and rear leg connecting plates. The aluminum frame is the robot's main body, and the rail-slider mechanism is mounted on the front end of the frame. The front leg connecting plate is fixed to the slider and can slide in the longitudinal direction of the frame, contributing to the linear structural DOF. The rear leg connecting plate is mounted at the frame's rear end. The front and rear motion modules are mounted on the front and rear leg connecting plates through front and rear hip rotation motors, respectively. The vehicle body module provides a mounting platform for the battery, control board, linear position sensor, Inertial Measurement Unit (IMU), and other equipment.

The front and rear motion modules have the same structure and consist of a hip rotation motor, a hip flexion motor, a knee joint motor, a wheel with a hub motor, a thigh, and a shank. The hip rotation motor located at the top of the motion module is used as the steering actuator. The hip flexion motor is mounted perpendicularly under the hip rotation motor and connected to the knee joint motor via the thigh. The knee joint motor is connected to the hub motor via the shank. The hub motor drives the wheel and controls the robot's speed.

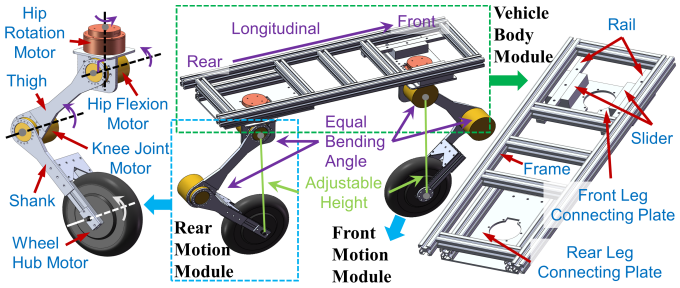

Fig. 1. Structure and composition of the two-wheeled robot.

The motion module can perform extension and retraction motions using the hip flexion and knee joint motors, which will be used in future work for jumping motions. In this study, the two motors hold the same bending angle during robot motions so that the frame height is constant and the wheel center coincides with the hip rotation motor axis.

B. Electrical Design

The electrical hardware of the multimodal two-wheeled robot in this work consists of eight different motors, one linear position sensor, one IMU, one Raspberry Pi 4 Model B with a CAN HAT, and lithium batteries. Two ends of the linear position sensors are mounted on the frame and the front leg, respectively, to measure the relative longitudinal displacement between them. The IMU can be used to measure the vehicle orientations in the future but will not be used in this work. The motors and linear position sensors communicate with the Raspberry Pi via a CAN bus while the IMU uses serial communication, as shown in Fig. 2. All electrical hardware is powered by lithium batteries.

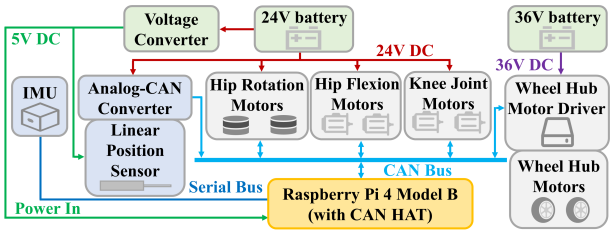

Fig. 2. Overview of electrical hardware architecture.

III. Kinematic Analysis

In this section, a general planar-motion kinematic model of the two-wheeled robot is developed, kinematics of the bicycle, self-balancing vehicle, and oblique vehicle are established, and the mode transformation procedure is presented.

A. Configuration description

Angles of the thigh and shank of the front motion module with respect to the hip rotation motor axis are denoted as θ_{ft}, θ_{fs}, respectively, and those of the rear motion module are θ_{rt}, θ_{rs}, respectively. The four angles are constant $\theta_{ft} = \theta_{fs} = \theta_{rt} = \theta_{rs} = \theta_0$ during robot movement. Therefore, the wheel centers coincide with the hip rotation motor axes, and the distance h is constant, as shown in Fig. 3. As a result,

the two legs behave as rigid bodies with only the steering control of their hip rotation motors. The center of the rail F_0 is set as the reference point of the front motion module, whose length from the axis of the rear hip rotation motor is a constant L. The distance from the hip flexion motor axis to the frame plane is a, the lengths of the thighs and shanks are b, and the wheel radius is r_w. Geometric relationship indicates $h = 2b\cos\theta_0$.

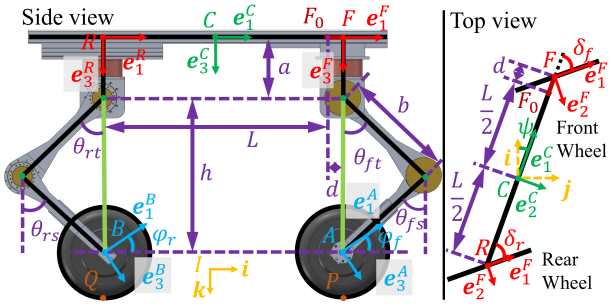

Fig. 3. Schematics of the coordinate systems and parameters of the robot.

Here, right-handed coordinate systems are used for the two-wheeled robot. The inertial coordinate system $\mathcal{F}^I = \{I; \boldsymbol{i}, \boldsymbol{j}, \boldsymbol{k}\}$ is fixed to the ground, where $\boldsymbol{k}$ is vertically downward and $\boldsymbol{i}$ point from the rear to the front, as shown in Fig. 3. In $\mathcal{F}^I$, coordinate system $\mathcal{F}^C = \{C; \boldsymbol{e}_1^C, \boldsymbol{e}_2^C, \boldsymbol{e}_3^C\}$, is fixed at the center of mass of the frame C with $\boldsymbol{r}_{IC} = x_c\boldsymbol{i} + y_c\boldsymbol{j} + (a + h + r_w)\,\boldsymbol{k}$, the vectors $\boldsymbol{e}_1^C$ and $\boldsymbol{e}_3^C$ are along the longitudinal axis of the frame and downward direction, respectively. The coordinate systems $\mathcal{F}^F = \{F; \boldsymbol{e}_1^F, \boldsymbol{e}_2^F, \boldsymbol{e}_3^F\}, \mathcal{F}^R = \{R; \boldsymbol{e}_1^R, \boldsymbol{e}_2^R, \boldsymbol{e}_3^R\}$ for the front and rear legs are fixed at F, R with $\boldsymbol{r}_{CF} = (L/2 + d)\,\boldsymbol{e}_1^C$, $\boldsymbol{r}_{CR} = -(L/2)\,\boldsymbol{e}_1^C$, where d is the offset of the front leg with respect to F_0, vectors $\boldsymbol{e}_2^F$, $\boldsymbol{e}_2^R$ are along the axes of their hip flexion motors and vectors $\boldsymbol{e}_3^F$, $\boldsymbol{e}_3^R$ point downward. The coordinate system $\mathcal{F}^A = \{A; \boldsymbol{e}_1^A, \boldsymbol{e}_2^A, \boldsymbol{e}_3^A\}$, $\mathcal{F}^B = \{B; \boldsymbol{e}_1^B, \boldsymbol{e}_2^B, \boldsymbol{e}_3^B\}$ for front and rear wheels are fixed at the wheel centers with $\boldsymbol{r}_{FA} = (a + h)\boldsymbol{e}_3^F, \boldsymbol{r}_{FB} = (a + h)\boldsymbol{e}_3^B$.

The contact points of the front and rear wheels on the ground are P and Q. This work focuses on the balanced planar motion of the two-wheeled robot so that the robot inclination angle is assumed to be zero. Therefore, the vectors $\boldsymbol{k}, \boldsymbol{e}_3^C, \boldsymbol{e}_3^F, \boldsymbol{e}_3^R$ are along the vertical direction, and the vectors $\boldsymbol{e}_2^F, \boldsymbol{e}_2^R$ and vectors $\boldsymbol{e}_2^A, \boldsymbol{e}_2^B$ are parallel, respectively. This condition is realized in this work by auxiliary wheels, which will be replaced using active balance control in future studies. The contact points P, Q are at $\boldsymbol{r}_{AP} = r_w\boldsymbol{e}_3^F$, $\boldsymbol{r}_{BQ} = r_w\boldsymbol{e}_3^R$ in frame $\mathcal{F}^A$ and $\mathcal{F}^B$, respectively.

The yaw angle of the robot, the steering angles of the front and rear legs, and the rotation angles of the front and rear wheels are denoted as ψ, δ_f, δ_r, φ_f, φ_r, respectively. At the initial state, we have $\psi = 0$, $d = 0, \delta_f = \delta_r = 0$, $\dot{\varphi}_f = \dot{\varphi}_r = 0$, so that vectors $\boldsymbol{e}_2^C$, $\boldsymbol{e}_2^F$, $\boldsymbol{e}_2^R$, $\boldsymbol{j}$, vectors $\boldsymbol{e}_2^F, \boldsymbol{e}_2^A$ and vectors $\boldsymbol{e}_2^R, \boldsymbol{e}_2^B$ are parallel to each other. In general, the homogeneous transformation matrix between $\mathcal{F}^X$, $\mathcal{F}^Y$ is denoted by T^{XY} with $X, Y \in \{I, C, F, R, A, B\}$. The translation vectors of $T^{IC}, T^{CF}, T^{CR}, T^{FA}, T^{RB}$ are $[x_c, y_c, a + h + r_w]^T$, $[L/2 + d, 0, 0]^T$, $[-L/2, 0, 0]^T$, $[0, 0, -a - h]^T$, $[0, 0, -a - h]^T$ and the rotation matrices are $R_3^I(\psi)$, $R_3^C(\delta_f)$, $R_3^C(\delta_r)$, $R_2^F(\varphi_f)$, $R_2^R(\varphi_r)$, respectively, in which $R_i^X(\alpha)$, $i = 1, 2, 3$ represents the rotation around the axis $\boldsymbol{e}_i^X$ in $\mathcal{F}^X$ by α.

B. Kinematic Modelling

1) Forward Kinematics: Assuming the wheels have no slippage, there are two velocity constrain equations at each road contact points P, Q, and their position are

$$\boldsymbol{r}_{IP} = \boldsymbol{r}_{IC} + \boldsymbol{r}_{CF} + \boldsymbol{r}_{FA} + \boldsymbol{r}_{AP} \tag{1}$$

$$\boldsymbol{r}_{IQ} = \boldsymbol{r}_{IC} + \boldsymbol{r}_{CR} + \boldsymbol{r}_{RB} + \boldsymbol{r}_{BQ} \tag{2}$$

Contact point velocities are the derivatives of their positions $\boldsymbol{v}_P = \dot{\boldsymbol{r}}_{IP}$, $\boldsymbol{v}_Q = \dot{\boldsymbol{r}}_{IQ}$. The contact point velocity for a wheel without slippage should be equal to $\boldsymbol{0}$. Therefore, the nonholonomic constraint equations can be obtained by combining the transformation relationship of coordinate systems:

$$\begin{aligned}\boldsymbol{v}_P =& \dot{\boldsymbol{r}}_{IC} + \dot{\boldsymbol{r}}_{CF} + \dot{\boldsymbol{r}}_{FA} + \dot{\boldsymbol{r}}_{AP} \\ =& \left(\dot{\tilde{x}}_c + \dot{d} + r_w\dot{\varphi}_f\cos(\delta_f)\right)\boldsymbol{e}_1^C \\ &+ \left(\dot{\tilde{y}}_C + \left(\frac{L}{2} + d\right)\dot{\psi} + r_w\dot{\varphi}_f\sin(\delta_f)\right)\boldsymbol{e}_2^C = \boldsymbol{0}\end{aligned} \tag{3}$$

$$\begin{aligned}\boldsymbol{v}_Q =& \dot{\boldsymbol{r}}_{IC} + \dot{\boldsymbol{r}}_{CR} + \dot{\boldsymbol{r}}_{RB} + \dot{\boldsymbol{r}}_{BQ} \\ =& \left(\dot{\tilde{x}}_c + r_w\dot{\varphi}_r\cos(\delta_r)\right)\boldsymbol{e}_1^C \\ &+ \left(\dot{\tilde{y}}_c - \frac{L}{2}\dot{\psi} + r_w\dot{\varphi}_r\sin(\delta_r)\right)\boldsymbol{e}_2^C = \boldsymbol{0}\end{aligned} \tag{4}$$

where $\dot{\tilde{x}}_c$, $\dot{\tilde{y}}_c$ are robot velocity components in $\mathcal{F}^C$. Due to the orthogonality of $\boldsymbol{e}_1^C$, $\boldsymbol{e}_2^C$, the above constraint equations are equivalent to four algebraic equations. Thus, the forward kinematic equations for the two-wheeled robot can be obtained by solving those equations:

$$\begin{bmatrix}\dot{\tilde{x}}_c \\ \dot{\tilde{y}}_c \\ \dot{\psi} \\ \dot{d}\end{bmatrix} = \begin{bmatrix}0 & -r_w\cos(\delta_r) \\ \frac{-L}{2L+2d}r_w\sin(\delta_f) & \frac{-L-2d}{2L+2d}r_w\sin(\delta_r) \\ \frac{-r_w}{L+d}\sin(\delta_f) & \frac{r_w}{L+d}\sin(\delta_r) \\ -r_w\cos(\delta_f) & r_w\cos(\delta_r)\end{bmatrix}\begin{bmatrix}\dot{\varphi}_f \\ \dot{\varphi}_r\end{bmatrix} \tag{5}$$

The equation gives the kinematic relationship between the workspace and configuration space of the two-wheeled robot, where the workspace includes three DOFs of planar motion $\dot{\tilde{x}}_c, \dot{\tilde{y}}_c, \dot{\psi}$ and one structural DOF $\dot{d}$, and the configuration space consists of four control inputs, namely, front and rear steering angles δ_f, δ_r and wheel speeds $\dot{\varphi}_f, \dot{\varphi}_r$.

The front leg origin F is desired to remain at initial position F_0, i.e., $d = 0$. Substituting this equation and its derivative $\dot{d} = 0$ into the forward kinematic equations yields

$$\begin{bmatrix}\dot{\tilde{x}}_c \\ \dot{\tilde{y}}_c \\ \dot{\psi}\end{bmatrix} = \begin{bmatrix}0 & -r_w\cos(\delta_r) \\ -\frac{r_w}{2}\sin(\delta_f) & -\frac{r_w}{2}\sin(\delta_r) \\ -\frac{r_w}{L}\sin(\delta_f) & \frac{r_w}{L}\sin(\delta_r)\end{bmatrix}\begin{bmatrix}\dot{\varphi}_f \\ \dot{\varphi}_r\end{bmatrix} \tag{6}$$

$$\dot{\varphi}_f\cos(\delta_f) = \dot{\varphi}_r\cos(\delta_r) \tag{7}$$

where (6) represents the relationship between the planar-motion workspace and the robot's configuration space, and

(7) is the servo constraint needed to maintain $d = 0$. The physical meaning of (7) is that the velocity components of the front wheel and the rear wheel along the longitudinal axis of the frame are the same.

2) Inverse Kinematics with Servo Constraint: Solving the control inputs from the forward kinematics equations yields the inverse kinematics equations:

$$\delta_f = \arctan\left(\frac{\dot{\tilde{y}}_c + \frac{1}{2}L\dot{\psi}}{\dot{\tilde{x}}_c}\right) \tag{8}$$

$$\delta_r = \arctan\left(\frac{\dot{\tilde{y}}_c - \frac{1}{2}L\dot{\psi}}{\dot{\tilde{x}}_c}\right) \tag{9}$$

$$\dot{\varphi}_f = -\frac{1}{r_w}\left(\dot{\tilde{x}}_c^2 + \left(\dot{\tilde{y}}_c + \frac{1}{2}L\dot{\psi}\right)^2\right)^{\frac{1}{2}} \tag{10}$$

$$\dot{\varphi}_r = -\frac{1}{r_w}\left(\dot{\tilde{x}}_c^2 + \left(\dot{\tilde{y}}_c - \frac{1}{2}L\dot{\psi}\right)^2\right)^{\frac{1}{2}} \tag{11}$$

These equations give control inputs for four configuration DOFs to achieve the three-DOF planar motion of the robot and satisfy the structural DOF servo constraint.

C. Multimodal Kinematics and Transformations

As shown in Fig. 4, the two-wheeled robot can exhibit three different specific motion modes, namely bicycle, self-balancing vehicle, and oblique vehicle, where the oblique vehicle mode is used to bridge the transformation between bicycle and self-balancing vehicle. The forward and inverse kinematic equations of three modes can be obtained by adding different additional servo constraints to that of the general two-wheeled robot.

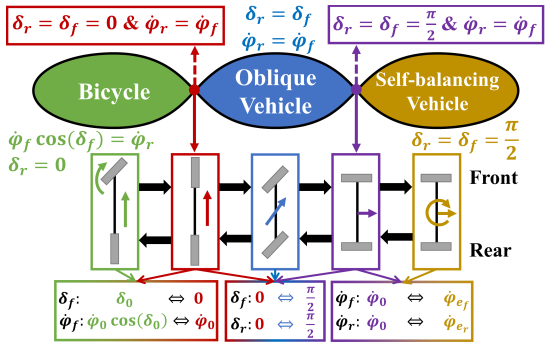

Fig. 4. Three specific modes of the robot and the mode transformation procedure. The symbols $\delta_f, \delta_r, \dot{\varphi}_f, \dot{\varphi}_r$ are steering angles of the front and rear legs and speeds of the front and rear wheels.

1) Bicycle: The rear leg steering angle in the bicycle mode remains unchanged at 0, so the additional constraint equation is $\delta_r = 0$. The forward kinematics is

$$\begin{bmatrix} \dot{\tilde{x}}_c \\ \dot{\tilde{y}}_c \\ \dot{\psi} \end{bmatrix} = \begin{bmatrix} -r_w\dot{\varphi}_r \\ -\frac{1}{2}r_w \sin(\delta_f)\,\dot{\varphi}_f \\ -\frac{r_w}{L}\sin(\delta_f)\,\dot{\varphi}_f \end{bmatrix} \tag{12}$$

$$\dot{\varphi}_f \cos(\delta_f) = \dot{\varphi}_r \tag{13}$$

The equations indicate that the robot's yaw angular velocity $\dot{\psi}$ and lateral translation velocity $\dot{y}$ are not independent but satisfy $L\dot{\psi} = 2\dot{\tilde{y}}_c$. Thus, the robot can only perform two-DOF planar motion by satisfying the servo constraints. Taking $\dot{\tilde{x}}_c$ and $\dot{\psi}$ as two independent motion control objectives of the inverse kinematics, the control inputs of the bicycle mode are

$$\delta_f = \arctan\left(\frac{L\dot{\psi}}{\dot{\tilde{x}}_c}\right) \tag{14}$$

$$\dot{\varphi}_f = -\frac{1}{r_w}\left(\dot{\tilde{x}}_c^2 + L^2\dot{\psi}^2\right)^{\frac{1}{2}} \tag{15}$$

$$\dot{\varphi}_r = -\frac{\dot{\tilde{x}}_c}{r_w} \tag{16}$$

2) Self-balancing Vehicle: In the self-balancing vehicle mode, the two wheels are kept perpendicular to the frame so that the additional constraint equations are $\delta_f = \delta_r = \frac{\pi}{2}$. Since $\cos(\delta_f) = \cos(\delta_r) = 0$, the wheels have no velocity component along the direction of the frame, and thus the structural servo constraints are naturally satisfied. The forward kinematic equations are

$$\begin{bmatrix} \dot{\tilde{x}}_c \\ \dot{\tilde{y}}_c \\ \dot{\psi} \end{bmatrix} = \begin{bmatrix} 0 \\ -\frac{1}{2}r_w\left(\dot{\varphi}_r + \dot{\varphi}_f\right) \\ \frac{r_w}{L}\left(\dot{\varphi}_r - \dot{\varphi}_f\right) \end{bmatrix} \tag{17}$$

Thus, the robot can only translate along $\boldsymbol{e}_2^C$. Its rotation is achieved by the differential speeds of the two wheels. Taking the lateral translation velocity $\dot{\tilde{y}}_c$ and rotation speed $\dot{\psi}$ as two independent motion control objectives, the expressions of the two control inputs are

$$\dot{\varphi}_f = -\frac{2\dot{\tilde{y}}_c + L\dot{\psi}}{2r_w} \tag{18}$$

$$\dot{\varphi}_r = -\frac{2\dot{\tilde{y}}_c - L\dot{\psi}}{2r_w} \tag{19}$$

3) Oblique Vehicle: In the oblique vehicle mode, the two legs can be steered to any equal angle with the additional constraint as $\delta_f = \delta_r$. Taking δ_r and $\dot{\varphi}_r$ as control inputs, the forward kinematic equations are

$$\begin{bmatrix} \dot{\tilde{x}}_c \\ \dot{\tilde{y}}_c \\ \dot{\psi} \end{bmatrix} = \begin{bmatrix} -r_w\dot{\varphi}_r\cos(\delta_r) \\ -r_w\dot{\varphi}_r\sin(\delta_r) \\ 0 \end{bmatrix} \tag{20}$$

and the structural servo constraint becomes

$$\dot{\varphi}_f = \dot{\varphi}_r \tag{21}$$

The robot can perform two-DOF translation motion while holding the structural servo constraint, and the yaw angle of the frame remains constant. Taking $\dot{\tilde{x}}_c$ and $\dot{\tilde{y}}_c$ as independent motion control objectives, the control inputs for the oblique vehicle are

$$\dot{\varphi}_f = \dot{\varphi}_r = -\frac{\left(\dot{\tilde{x}}_c^2 + \dot{\tilde{y}}_c^2\right)^{\frac{1}{2}}}{r_w} \tag{22}$$

$$\delta_f = \delta_r = \arctan\left(\frac{\dot{\tilde{y}}_c}{\dot{\tilde{x}}_c}\right) \tag{23}$$

4) Mode Transformation: There are overlaps between the configuration space of the oblique vehicle mode and those of the bicycle and self-balancing vehicle modes, as shown in Fig. 4. Thus, transformations between the bicycle and self-balancing vehicle can be implemented by the oblique vehicle mode, where the constraint $d = 0$ is automatically satisfied. When $\delta_f = \delta_r = 0$, $\dot{\varphi}_f = \dot{\varphi}_r$, the robot is in both bicycle and oblique vehicle modes. When $\delta_f = \delta_r = \pi/2$, $\dot{\varphi}_f = \dot{\varphi}_r$, the robot is in both self-balancing vehicle and oblique vehicle modes.

The transformation procedure from bicycle to self-balancing vehicle with the oblique vehicle as the transition state is given below, and the procedure from the self-balancing vehicle to bicycle is the reverse. Without loss of generality, the control inputs in the bicycle mode at the beginning of the transformation are $\delta_f = \delta_0, \delta_r = 0, \dot{\varphi}_f = \dot{\varphi}_0/\cos(\delta_0), \dot{\varphi}_r = \dot{\varphi}_0$, and the control inputs in the self-balancing vehicle mode at the end of transformation are $\delta_f = \frac{\pi}{2}, \delta_r = \frac{\pi}{2}, \dot{\varphi}_f = \dot{\varphi}_{e_f}, \dot{\varphi}_r = \dot{\varphi}_{e_r}$. The transformation procedure is given: 1) In Step 1, the rear leg angle $\delta_r = 0$ and the rear wheel rotational speed $\dot{\varphi}_r = \dot{\varphi}_0$ are constant, and the front leg angle $\delta_f = 0$ is steered from δ_0 to 0 while the front wheel rotational speed $\dot{\varphi}_f$ is adjusted with $\dot{\varphi}_f = \dot{\varphi}_0/\cos(\delta_f)$; 2) In Step 2, the front and rear wheel rotational speeds $\dot{\varphi}_f = \dot{\varphi}_r = \dot{\varphi}_0$ are constant, and the front and rear leg steering angles $\delta_f = \delta_r$ are gradually steered from 0 to $\pi/2$; 3) In Step 3, the front and rear leg rotation angles $\delta_f = \delta_r = \frac{\pi}{2}$ are constant, and the front and rear wheel rotational speeds $\dot{\varphi}_f$, $\dot{\varphi}_r$ gradually changes from $\dot{\varphi}_0$ to $\dot{\varphi}_{e_f}$,$\dot{\varphi}_{e_r}$, respectively.

IV. Results

A. Prototype

A prototype is developed to validate the proposed method of motion mode transformation for the two-wheeled robot. As shown in Fig. 5, the outer size of the aluminum frame is $800\,\mathrm{mm} \times 260\,\mathrm{mm}$. Two hip rotation motors (MF9025V2, Shanghai Lingkong Technology) with a maximum torque of $5.8\,\mathrm{Nm}$ are initially spaced at a distance of $L = 500\,\mathrm{mm}$. The hip flexion leg motor (M8010E17B50, HangZhou YiZhi Technology) is of the same model as the knee joint motor, with a maximum output torque of $34\,\mathrm{Nm}$, and can be locked at a fixed angle when energized. Limited by the length of the rail and the frame, the relative displacement d takes the value in the range of $d \in [-30\,\mathrm{mm}, 30\,\mathrm{mm}]$. The linear position sensor (KTM150mm, WXXY Millay) with a range of $150\,\mathrm{mm}$ and an accuracy of $\pm 0.01\,\mathrm{mm}$ can cover the slider range. A $36\,\mathrm{V}$ lithium battery and a $24\,\mathrm{V}$ lithium battery are mounted in the center above the frame, with the former used to power the hub motors (ZLLG80ASM250, Shenzhen ZhongLing Technology) and the latter used to power the rest of the electrical components. The IMU (N100 Mini, Wheeltec) is mounted directly below the frame's geometric center. The geometry parameters of the motion module are $a = 136\,\mathrm{mm}$, $b = 250\,\mathrm{mm}$, $r_w = 100\,\mathrm{mm}$, and the hub motor has a rated torque of $4\,\mathrm{Nm}$ and a maximum speed of $500\,\mathrm{rpm}$. All motors have servo control functions for rotation angle and angular speed. An auxiliary support bracket is mounted around the body to keep the robot balanced, where omnidirectional wheels (R2-0905-60-001, Rotacaster) are installed at the bottom. The support prevents the robot from tilting but does not constrain its planar DOFs.

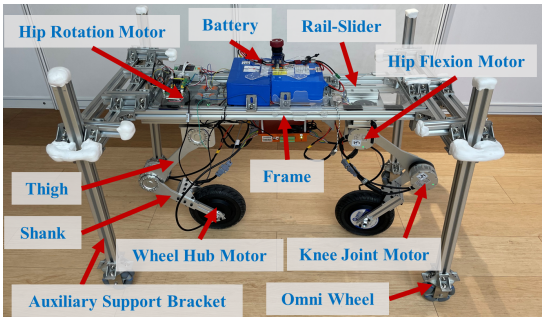

Fig. 5. Prototype of the two-wheeled robot.

B. Experiments

This subsection shows the experimental results of motions in three modes and configuration transformation experiments using the prototype. During testing, the bending angles of the hip flexion and knee joint motors are $\theta_0 = 45°$, the height of the frame from the ground is $a + h = 490\,\mathrm{mm}$, and the front and rear wheel turning angle ranges are $\delta_f, \delta_r \in [-\pi/2, \pi/2]$.

1) Bicycle mode: In the bicycle mode, the rear wheel's rotation speed $\dot{\varphi}_r$ and the front wheel steering angle δ_f are used to control the moving speed and direction of the robot, respectively. The target $d = 0$ of the structural DOF is controlled by the front wheel rotation speed $\dot{\varphi}_f$, which increases when $d < 0$ and decreases when $d > 0$. The control law is

$$\dot{\varphi}_f = \dot{\varphi}_f^{Ref} - \frac{K_1^p}{\cos\left(\max\left(|\delta_f|, \frac{\pi}{3}\right)\right)} d \tag{24}$$

where the first term $\dot{\varphi}_f^{Ref} = \dot{\varphi}_r \cos(\delta_f)$ at the right hand is the control reference obtained by (13), and the second term is the feedback control term, in which $K_1^p = 0.75\,\mathrm{rpm/mm}$ is the nominal proportion coefficient, and d is the measured slider displacement. The function $\cos(\delta_f)$ is used as nonlinear corrections to the nominal proportion coefficient, and the angular limit $|\delta_f| \leq \pi/3$ is applied to prevent singularity. In the bicycle mode experiment, the robot sequentially performs motions of a straight movement, right turn, left turn, and back to the straight. The configuration space and workspace coordinates are shown in Fig. 6 (a)∼(c), where $|d| \leq 3\,\mathrm{mm}$ implies that the control law (24) can keep the structural DOF stabilized during the motion.

2) Self-balancing vehicle mode: In self-balancing vehicle mode, the front and rear wheel speeds $\dot{\varphi}_f, \dot{\varphi}_r$ are used to control the moving speed and direction of the robot together. Neither wheel has a velocity component along the longitudinal axis of the frame. Ideally, the structural DOF d always remains constant. However, it has been shown in the experiments that d changes rapidly when the robot rotates

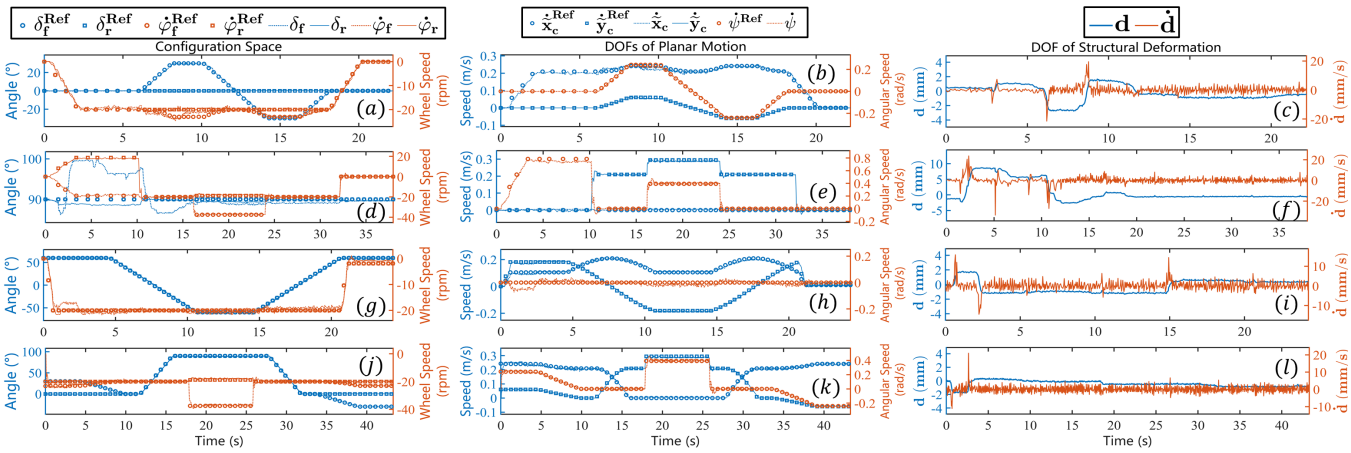

Fig. 6. Validation experiment results. The four rows represent the experimental results of the bicycle, self-balancing vehicle, oblique vehicle, and transformation motions from the top to the bottom. The three columns from the left to the right are time histories of the configuration space coordinates, three DOFs of planar motions, and the structural DOF. The legends of each column are located at the top of the column, in which δ_f^{Ref}, δ_r^{Ref}, $\dot{\varphi}_f^{Ref}$, $\dot{\varphi}_r^{Ref}$ are reference values given by inverse kinematics, and δ_f, δ_r, $\dot{\varphi}_f$, $\dot{\varphi}_r$ are values measured during experiments. $\dot{\tilde{x}}_c^{Ref}, \dot{\tilde{y}}_c^{Ref}, \dot{\psi}^{Ref}$ are planned value for the planar motion, while $\dot{\tilde{x}}_c, \dot{\tilde{y}}_c, \dot{\psi}$ are experimental values obtained by measurements. The measured value matches the reference value well. d and $\dot{d}$ are measured values of structural DOF and are stable under control. The horizontal axes are labeled at the bottom.

around its mass center, which is caused by centrifugal force. Therefore, a control law is designed to balance the effect of centrifugal force and keep d constant by utilizing the offset of the front wheel steering angle:

$$\delta_f = \delta_f^{Ref} - K_2^p \operatorname{sgn}(\dot{\varphi}_f)\, d \tag{25}$$

where $\delta_f^{Ref} = \pi/2$ is the reference of the front wheel steering angle, $K_2^p = 1.25\,\mathrm{deg/mm}$ is the proportion coefficient of the feedback control term, sgn is the signum function and d is the measured value of the slider displacement. When $d \neq 0$, the front wheel angle deviates from $\pi/2$, making the wheel generate a recovery velocity component along the longitudinal direction of the frame. At the same time, wheel speed control is introduced to maintain the velocity component of the front wheel perpendicular to the longitudinal direction of the body at the desired value $\dot{\varphi}_f^{\perp Ref}$:

$$\dot{\varphi}_f = \dot{\varphi}_f^{\perp Ref} / \cos\left(\delta_f - \frac{\pi}{2}\right) \tag{26}$$

Since δ_f is near $\pi/2$, the above equation does not have singularities. In self-balancing vehicle motion experiments, the robot sequentially performs the motions of rotating 360° in place, moving forward, and turning around while moving forward. The configuration and workspace coordinates are shown in Fig. 6 (d)∼(f). The structural DOF $d \leq 3\,\mathrm{mm}$ during forwarding and large radius turning, but there is a significant steady-state error of d when the vehicle is spinning around its mass center, which is about $8\,\mathrm{mm}$. The reason is that the steady-state error is required in (25) to generate a non-zero value of δ_f to balance the centrifugal force.

3) Oblique vehicle mode: The two steering angles $\delta_f = \delta_r$ are used to control the robot's direction, and the two wheels' speeds $\dot{\varphi}_f^{Ref} = \dot{\varphi}_r$ are used to control the velocity of the robot in the oblique vehicle mode, where $\dot{\varphi}_f^{Ref}$ is the control reference given by kinematic equation (21). The velocity of the front wheel is also used to control the structural DOF d, and the control law is (24). The oblique vehicle is subjected to straight and turning motions in the experiment, and the experimental results are shown in Fig. 6 (g)∼(i). In steady state, the structural DOF $d \leq 2\,\mathrm{mm}$.

4) Transformation: Following the procedure in Section 3, the robot is transformed from a general configuration of the bicycle mode to that of the self-balancing vehicle mode and then inversely transformed back to another general configuration of the bicycle mode. The results of the transformation process are displayed in Fig. 6 (j)∼(l). The experimental results show that the robot can smoothly transform between the bicycle and self-balancing vehicle modes, and the structural DOF always satisfies $d \leq 2\,\mathrm{mm}$ during the process.

V. Conclusion

In this study, a two-wheeled robot that can smoothly switch between bicycle mode and self-balancing vehicle mode is designed. This robot incorporates one structural DOF to avoid the over-constraint problem induced by the four control inputs of the two steerable drive wheels. Meanwhile, a control law is developed to keep the structural DOF constant at different modes, and experimental results show the effectiveness of the control law. Based on the established kinematic models of the bicycle, self-balancing vehicle, and oblique vehicle, a procedure is designed to transform the bicycle and self-balancing vehicle modes by a transition mode of the oblique vehicle. The planar motion's kinematic properties and multimodal transformation capacity of the proposed two-wheeled robot are experimentally verified on a prototype with an auxiliary support bracket to keep the robot upright. Active balance control without the bracket will be studied in the future.

REFERENCES

[1] R. P. M. Chan, K. A. Stol, and C. R. Halkyard, "Review of modelling and control of two-wheeled robots," *Annual Reviews in Control*, vol. 37, no. 1, pp. 89–103, Apr. 2013.

[2] D. J. Limebeer and R. S. Sharp, "Bicycles, motorcycles, and models," *IEEE Control Systems Magazine*, vol. 26, no. 5, pp. 34–61, 2006.

[3] J. D. G. Kooijman, J. P. Meijaard, J. M. Papadopoulos, A. Ruina, and A. L. Schwab, "A Bicycle Can Be Self-Stable Without Gyroscopic or Caster Effects," *Science*, vol. 332, no. 6027, pp. 339–342, Apr. 2011.

[4] J. Xiong, N. Wang, and C. Liu, "Stability analysis for the Whipple bicycle dynamics," *Multibody System Dynamics*, vol. 48, no. 3, pp. 311–335, Mar. 2020.

[5] F. Grasser, A. D'Arrigo, S. Colombi, and A. Rufer, "JOE: A mobile, inverted pendulum," *IEEE Transactions on Industrial Electronics*, vol. 49, no. 1, pp. 107–114, Feb./2002.

[6] J. Xu, S. Shang, H. Qi, G. Yu, Y. Wang, and P. Chen, "Simulative investigation on head injuries of electric self-balancing scooter riders subject to ground impact," *Accident Analysis & Prevention*, vol. 89, pp. 128–141, Apr. 2016.

[7] G. Campion, G. Bastin, and B. Dandrea-Novel, "Structural properties and classification of kinematic and dynamic models of wheeled mobile robots," *IEEE transactions on robotics and automation*, vol. 12, no. 1, pp. 47–62, 1996.

[8] H. Taheri and C. X. Zhao, "Omnidirectional mobile robots, mechanisms and navigation approaches," *Mechanism and Machine Theory*, vol. 153, p. 103958, Nov. 2020.

[9] X. Yun and N. Sarkar, "Dynamic feedback control of vehicles with two steerable wheels," in *Proceedings of IEEE International Conference on Robotics and Automation*, vol. 4, Apr. 1996, pp. 3105–3110 vol.4.

[10] M. Mauder, "Robust tracking control of nonholonomic dynamic systems with application to the bi-steerable mobile robot," *Automatica*, vol. 44, no. 10, pp. 2588–2592, Oct. 2008.

[11] X. Meng, L. Guo, and Q. Liao, "Analysis of nonholonomic constraints about a variable structure bicycle robot," in *2012 IEEE International Conference on Automation and Logistics*. Zhengzhou, China: IEEE, Aug. 2012, pp. 628–633.

[12] T. D. Murphey and J. W. Burdick, "Issues in controllability and motion planning for overconstrained wheeled vehicles," in *Proc. Int. Conf. Math. Theory of Networks and Systems (MTNS)*. Citeseer, 2000.

[13] J. Borenstein, "Control and kinematic design of multi-degree-of freedom mobile robots with compliant linkage," *IEEE Transactions on Robotics and Automation*, vol. 11, no. 1, pp. 21–35, Feb./1995.

[14] P. F. Muir and C. P. Neuman, "Kinematic modeling of wheeled mobile robots," *Journal of robotic systems*, vol. 4, no. 2, pp. 281–340, 1987.

[15] R. Holmberg and O. Khatib, "Development and Control of a Holonomic Mobile Robot for Mobile Manipulation Tasks," *The International Journal of Robotics Research*, vol. 19, no. 11, pp. 1066–1074, Nov. 2000.

[16] D. Reister and M. Unseren, "Position and constraint force control of a vehicle with two or more steerable drive wheels," *IEEE Transactions on Robotics and Automation*, vol. 9, no. 6, pp. 723–731, Dec./1993.

[17] B. Thuilot, B. d'Aandrea-Novel, and A. Micaelli, "Modeling and feedback control of mobile robots equipped with several steering wheels," *IEEE Transactions on Robotics and Automation*, vol. 12, no. 3, pp. 375–390, June 1996.

[18] M. Wada, "Virtual link model for redundantly actuated holonomic omnidirectional mobile robots," in *Proceedings 2006 IEEE International Conference on Robotics and Automation, 2006. ICRA 2006.* Orlando, FL, USA: IEEE, 2006, pp. 3201–3207.

[19] A. Schiele and F. C. T. Van Der Helm, "Kinematic Design to Improve Ergonomics in Human Machine Interaction," *IEEE Transactions on Neural Systems and Rehabilitation Engineering*, vol. 14, no. 4, pp. 456–469, Dec. 2006.

[20] H.-C. Hsieh, D.-F. Chen, L. Chien, and C.-C. Lan, "Design of a Parallel Actuated Exoskeleton for Adaptive and Safe Robotic Shoulder Rehabilitation," *IEEE/ASME Transactions on Mechatronics*, vol. 22, no. 5, pp. 2034–2045, Oct. 2017.

[21] J. Pan, D. Astarita, A. Baldoni, F. Dell'Agnello, S. Crea, N. Vitiello, and E. Trigili, "NESM- γ : An Upper-Limb Exoskeleton With Compliant Actuators for Clinical Deployment," *IEEE Robotics and Automation Letters*, vol. 7, no. 3, pp. 7708–7715, July 2022.